Applied Science and Engineering Progress, Vol. 20, No. 4, 2027, 8390

Research Article

Valorization of Waste Cooking Oil via Co-Production of Fuel-Grade Biodiesel and Solid Bio-PCM Thermal Storage

Ahmad Zikri*, Martha Aznury, Rima Daniar, and Iriani Reka Septiana
Department of Chemical Engineering, Politeknik Negeri Sriwijaya, Palembang, South Sumatra, Indonesia

* Corresponding author. E-mail: ahmad.zikri@polsri.ac.id DOI: 10.14416/j.asep.2026.11.012
Received: 8 September 2026; Revised: 16 October 2026; Accepted: 20 October 2026; Published online: 25 November 2026
© 2026 King Mongkut's University of Technology North Bangkok. All Rights Reserved

Abstract
Waste cooking oil (WCO) is an abundant waste resource that is often poorly managed. Phase change materials (PCMs) derived from WCO are typically prepared from crude or lightly refined oil, resulting in broad and poorly defined melting ranges that fall below the indoor thermal-comfort range. In conventional biodiesel production, winterization improves cold-flow properties, while the crystallized saturated fraction is discarded as a yield loss. In this study, winterization is instead employed as a co-production step to obtain both biodiesel and a bio-based PCM (Bio-PCM) from a single batch of WCO. WCO was processed through a sequence of bleaching-earth pretreatment, acid-catalyzed esterification, base-catalyzed transesterification, and controlled low-temperature winterization. Bleaching with 3% (w/w) activated bleaching earth removed pigments but reduced the free fatty acid (FFA) content only from 7.22% to 5.60%. Subsequent esterification using 4.0 g of H_2SO_4 reduced the FFA content to 0.55 ± 0.09% (one-way ANOVA, F = 2735.69, *p*-value < 0.0001). Transesterification subsequently achieved a fatty acid methyl ester (FAME) yield of 94.60 ± 0.92% and an ester content of 97.53 ± 0.55%, both of which met the requirements of EN 14214 and SNI 7182. A single controlled cooling stage at 10–12 °C isolated a solid fraction equivalent to 33.22 ± 2.41% of the FAME mass. This fraction was enriched in saturated esters, whose proportion increased from 72.8% to 76.8%, and was dominated by methyl palmitate (29.23%) and methyl laurate (21.22%), as determined by GC–MS. Differential scanning calorimetry of five eutectic formulations containing the solid FAME fraction (Fs) and stearic acid (5–25 wt% stearic acid) showed that both the transition temperature and latent heat increased with stearic acid content. Under a nitrogen atmosphere, the blend containing 25 wt% stearic acid (P5) exhibited a melting range of 31.0–39.0 °C, making it potentially suitable for exterior building-envelope applications, such as roofs and sun-exposed walls. However, its latent heat was only 8.08 J/g under nitrogen and 28.08 J/g under air, substantially lower than that of commercial fatty-acid-based and paraffin-based PCMs. The possible causes of this low and variable latent heat, along with practical strategies for improvement, are discussed. This study establishes a statistically validated mass balance for converting a waste feedstock into a compositionally and thermally characterized Bio-PCM candidate and identifies the remaining performance gaps that must be addressed before the material can be used for passive thermal management of tropical building envelopes.

Keywords: Bio-based phase change material, Esterification, Fatty acid methyl ester, Waste cooking oil, Winterization

1 Introduction

Rapid urbanization and rising space-cooling demand have made buildings a major and growing consumer of energy, particularly in tropical countries such as Indonesia, where air-conditioning dominates the thermal energy budget of the building stock. Latent heat thermal energy storage using phase change materials (PCM) is an established strategy for damping this demand: a PCM absorbs excess heat during the day through melting and releases it during cooler periods through solidification, flattening indoor temperature swings and lowering the load on mechanical cooling [1].

Commercial PCM formulations remain dominated by paraffin waxes, which, despite favourable latent heat, suffer from flammability, fossil origin, high cost, and environmental persistence. Bio-based PCM (Bio-PCM) derived from vegetable oils, fatty acids, and their esters

Applied Science and Engineering Progress, Vol. 20, No. 4, 2027, 8390

have therefore attracted sustained interest, since many combine latent heat capacities adequate for building service temperatures with low toxicity, renewability, and biodegradability [2], [3]. Recent reviews of waste-valorized PCM further identify waste-derived feedstocks as the most credible route to cost parity with paraffin [4]-[6].

Among candidate feedstocks, waste cooking oil (WCO) is especially attractive: it is generated in large volumes as a household and industrial waste stream, poses a pollution risk when discharged untreated, and can be converted into fatty-acid-derived materials at a fraction of the cost of virgin bio-oils or fossil paraffin [7]. Several studies have demonstrated the feasibility of waste- and coconut-oil-based PCM for thermal storage and building-envelope integration, including encapsulated capsules in foamed concrete [8] and fatty-acid eutectic blends [9]. Fatty acid derivatives of WCO have likewise been processed directly into PCM for thermal storage systems [10].

Parallel progress on the fuel side has made WCO an increasingly attractive feedstock. Two-step acid–base processing is now routine for high-FFA lipids; for example, high-FFA crude palm kernel oil has been converted to biodiesel with 96.59% ester content [11], and response surface and process-simulation approaches have been used to optimize the methanol-to-oil ratio and catalyst loading of palm-derived biodiesel [12]. Ternary blends based on WCO biodiesel have been tested for performance and emissions in agricultural diesel engines [13], and biorefinery analyses show that WCO processing becomes economically attractive mainly when biodiesel is co-produced with a second value-added product, such as methyl ester sulfonate surfactants [14] or upgraded glycerol derivatives [15]. On the thermal-storage side, recent reviews emphasize that the PCM transition window must be matched to the application: melting points of about 24–30 °C are recommended for indoor comfort in warm climates [16]-[18], whereas roof and exterior-wall layers exposed to solar irradiance benefit from higher transitions, with organic PCMs melting at 35–37 °C reducing roof cooling loads by up to 69% in a hot climate [19]. Fatty-acid eutectics used for these purposes typically store 127–205 J/g and retain their properties over hundreds to thousands of melt–freeze cycles [20], [21]. A WCO process that delivers both fuel and a PCM co-product could therefore improve the economics of both streams, provided that the PCM fraction is matched to a defined building application.

Three limitations recur across this literature and jointly define the gap addressed here. First, feedstock is used unfractionated: most WCO-PCM studies employ crude or only lightly refined oil [10], which retains a broad and batch-variable mixture of saturated and unsaturated fatty acids and therefore melts over an ill-defined range that generally lies below the 20–30 °C indoor comfort window, limiting usable latent heat at service temperature. Second, FAME-based PCM work relies on purchased pure esters: studies that do achieve sharp, comfort-range transitions use commercial-grade methyl palmitate, methyl stearate, or their eutectics with fatty acids [22], [23], which establish the thermophysical case for methyl esters as PCM but say nothing about whether an equivalent fraction can be obtained from a waste feedstock, and whose reagent cost removes the economic advantage that motivates waste valorization. Third, the saturated crystal fraction is treated as a loss rather than a product: in biodiesel practice, winterization is applied specifically to remove long-chain saturated FAME in order to lower cloud and pour point, and the crystallized solid is reported as a yield penalty to be minimized or discarded [24], [25], yet to the authors' knowledge no study has isolated that crystallized fraction, characterized its composition, and evaluated it as a Bio-PCM in its own right. Consequently, there is no reported process chain that carries a single waste feedstock through to a compositionally characterized, near-ambient-melting Bio-PCM while simultaneously accounting for the fuel-grade co-product, and no closed mass balance quantifying how much PCM-grade material a given volume of WCO can yield.

This work addresses that gap through four specific contributions. First, process reframing repositions winterization from a fuel-quality corrective step to a deliberate fractionation stage, enabling a single WCO batch to yield two saleable products: a liquid FAME fraction obtained from EN 14214/SNI 7182-compliant biodiesel, and a solid, saturated-rich Bio-PCM candidate, rather than a fuel product and a waste stream. Second, a quantified single-stage enrichment is achieved: a single controlled cooling stage at 10–12 °C, without agitation or solvent-assisted crystallization, raises saturated FAME content from 72.8% to 76.8% and isolates 33.22 ± 2.41% of the FAME mass as a solid fraction, giving the first reported PCM-yield figure per unit of WCO processed by this route. Third, the chain is statistically validated and mass-balanced: every stage is replicated in triplicate and tested by one-way ANOVA with Tukey's HSD, and the transesterification stage is closed to 92.8% by mass with the FAME-to-glycerol ratio reconciled against reaction

stoichiometry, a level of process accounting largely absent from prior WCO-PCM reports. Fourth, a mechanistic interpretation of composition is offered: the retention of low-melting methyl laurate (melting point ≈ 5.2 °C) in a fraction crystallized at 10–12 °C is tentatively attributed to co-crystallization within the lattice nucleated by methyl palmitate and methyl stearate, which also explains why the fraction is expected to melt over a range rather than at a single point.

The specific objectives are to (i) establish bleaching, esterification, and transesterification conditions that convert WCO into high-purity FAME; (ii) isolate a saturated-FAME-rich solid fraction by controlled winterization and quantify its yield; (iii) characterize the fatty acid composition of that fraction by GC-MS and assess, on a compositional basis, its suitability as a Bio-PCM; and (iv) evaluate Fs–stearic acid blends by DSC and TGA and define the building application for which they are suited. The leading formulation is intended for exterior building envelopes (roof layers and sun-exposed wall panels), where surface temperatures in tropical climates reach 35–45 °C, whereas formulations for indoor comfort are treated as a tuning target. This work forms the first stage of a larger programme targeting a self-healing, microencapsulated smart-PCM for gypsum-based green building panels, a route for which encapsulated-PCM gypsum and cementitious systems provide the application precedent [26]-[30].

2 Materials and Methods

2.1 *Materials*

WCO was collected and used as the primary feedstock. Tianyu-brand activated bleaching earth was used for pretreatment. Analytical-grade methanol, sulfuric acid (H_2SO_4), potassium hydroxide (KOH), and deionized water were used for esterification and transesterification. All chemicals were used as received.

The two catalysts were selected for specific reasons. Because the bleached oil still contained 5.60% FFA, well above the approximately 1–2 wt% tolerated by alkaline catalysts [31], a homogeneous Brønsted acid was needed first; concentrated H_2SO_4 is inexpensive, highly active for FFA esterification at 60 °C, and also acts as a dehydrating agent that binds the water formed, shifting the equilibrium toward methyl esters [32], [11]. For the second step, KOH was preferred over NaOH because it dissolves faster and more completely in methanol to form potassium methoxide, gives faster transesterification [31], and forms potassium soaps that are more soluble and less prone to gelling than sodium soaps, which eases FAME–glycerol phase separation. The acid–base two-step sequence is the standard configuration for high-FFA feedstocks in recent optimization studies [12], [11].

2.2 *Bleaching pretreatment*

Crude WCO was filtered to remove macroscopic impurities. Bleaching earth was added at 1% (S1), 2% (S2), and 3% (S3) w/w, and the mixture was stirred at 400 rpm and 80 °C for 30 min; an untreated sample (M0) served as the control. Oil mass and yield were recorded gravimetrically, and FFA content was determined by acid-base titration with KOH (Figure 1a), from which the acid value was calculated. All measurements were performed in triplicate.

2.3 *Acid-catalyzed esterification*

Bleached oil (S3, FFA = 5.60%) was reacted with methanol (45.0 g) and concentrated H_2SO_4 at 2.0 g (S4), 3.0 g (S5), and 4.0 g (S6) at 60 °C and 400 rpm for 60 min, followed by 60 min of gravity phase separation (Figure 1b). Oil mass, yield, FFA, acid value, kinematic viscosity (Ostwald viscometer, 30°C), density (pycnometer), and colour absorbance (470 nm) were determined in triplicate.

2.4 *Base-catalyzed transesterification*

The esterified oil with the lowest FFA (S6, 0.55 ± 0.09%) was reacted at 170 g scale with potassium methoxide (1.7 g KOH in 30 g methanol; methanol-to-oil molar ratio ≈ 4.1:1, based on a mean triglyceride molar mass of ≈ 738 g/mol calculated from the GC-MS composition) at 60–63°C and 500 rpm for 120 min. The mixture was separated into FAME and glycerol phases for 8–12 h, and the FAME layer was washed with warm deionized water to neutral pH (6.5–7.0). FAME yield, density (ASTM D1480, 40°C), ester content (EN 14103/^{1}H-NMR), acid value (AOCS Cd 3d-63), kinematic viscosity (ASTM D445, 40°C), and glycerol by-product mass were determined in triplicate. After reaction, the FAME and glycerol phases were separated in a separatory funnel and the FAME layer was washed in the same way (Figure 1c, d).

Applied Science and Engineering Progress, Vol. 20, No. 4, 2027, 8390

2.5 *Winterization (fractionation of saturated FAME)*

Purified FAME was cooled at approximately 1 °C per 5 min to a crystallization temperature of 10–12 °C and held without agitation for 24 h in a temperature-controlled cooling cabinet (Figure 1e). The solid fraction (Fs, the candidate Bio-PCM) was separated from the residual liquid fraction (Fl) by vacuum filtration at controlled temperature, with the filtration unit kept inside the cabinet (Figure 1f), and washed with cold methanol. Yields of Fs and Fl relative to total FAME feed (F) were determined gravimetrically in triplicate. The cake was washed once with cold methanol; the wash volume and temperature were not optimized in this first study.

2.6 *Compositional and statistical analysis*

The FAME composition of F, Fs, and Fl was determined by GC-MS, and individual esters were classified as saturated (SFAME) or unsaturated (UFAME) from peak identity and retention time. Differences among treatment groups were evaluated by one-way ANOVA followed by Tukey's HSD post-hoc test at a 95% confidence level.

Because GC-MS peak areas were obtained from the total-ion current without response-factor correction, the reported compositions are relative and semi-quantitative. All process measurements were made in triplicate and are reported as mean ± standard deviation (SD, n = 3). In all figures, error bars denote ± 1 SD, and means that do not share a letter differ significantly (Tukey's HSD, p-value < 0.05).

2.7 *Preparation and thermal analysis of Fs–stearic acid blends*

Five blends were prepared from 5 g of Fs and stearic acid at 5, 10, 15, 20 and 25 wt% of the blend (P1–P5) using a high-speed homogeniser (Figure 1h) and were stored in closed containers at room conditions (Figure 1i); the samples sent for thermal analysis are shown in Figure 1j. Thermal analyses were carried out at the Integrated Research and Testing Laboratory (LPPT), Universitas Gadjah Mada. DSC of P1–P5 (2.45–3.88 mg; Test Report No. MP-260801002678) was performed by heating the samples in sealed aluminium pans on a DSC-60 Plus (Shimadzu) at 10 °C/min under an air purge of 10 mL/min; data were recorded from about 20 °C to 300 °C. P3 and P4 (12.0–12.7 mg) were also analysed by simultaneous TGA–DTA (DTG-60, Shimadzu) from 30 to 300 °C at 10 °C/min. P3 and P5 (4.51 and 4.82 mg; Test Report No. MP-261001003203) were also analysed under nitrogen (10 mL/min) in sealed aluminium pans, heated from 10 to 80 °C at 10 °C/min and held for 5 min at 80 °C. Onset, peak and endset temperatures and the enthalpy of melting (ΔH) were obtained with the instrument software using a linear baseline drawn across the endotherm, and the integration was checked independently from the exported raw data.

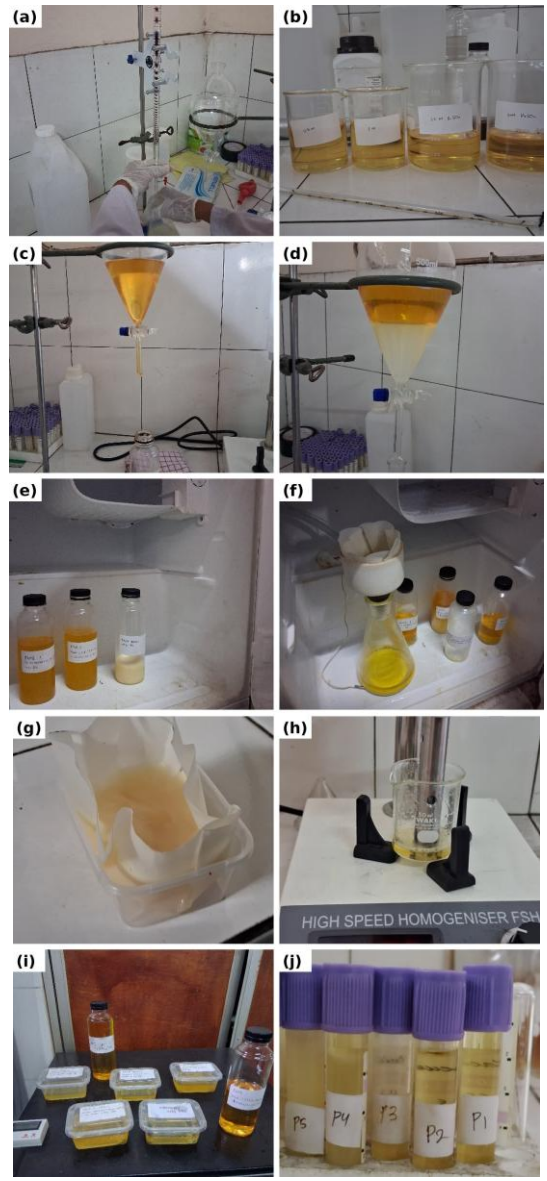


Figure 1: Photographs of the main experimental steps: (a) titration of free fatty acids; (b) oil after acid-catalyzed esterification with different H_2SO_4 doses; (c) separation of the FAME and glycerol phases after base-catalyzed transesterification; (d) washing of the FAME layer with

warm deionized water; (e) FAME held in the cooling cabinet at 10–12°C during winterization; (f) vacuum filtration of the crystallized fraction inside the cabinet; (g) the solid fraction Fs; (h) blending of Fs with stearic acid in a high-speed homogeniser; (i) Fs–stearic acid blends stored at room conditions next to a thermo-hygrometer; (j) sample vials of blends P1–P5 prepared for DSC and TGA characterization.

3 Results and Discussion

3.1 *Bleaching pretreatment*

Yield decreased systematically from 100% (M0) to 98.80% (S3), and the mass lost at each dose was consistently equal to 40% of the bleaching earth added (Table 1). This proportionality indicates that oil loss was governed by mechanical retention within the spent adsorbent cake rather than by evaporation or thermal degradation, consistent with reports identifying spent bleaching earth as the principal source of oil loss in vegetable-oil refining [33].

FFA fell from 7.22 ± 0.10% to only 5.60 ± 0.10% at 3% BE, a 22.4% reduction (Table 2, Figure 2). One-way ANOVA confirmed a significant effect of bleaching-earth dose ($F = 149.71$, p-value < 0.001), although S1 and S2 were statistically indistinguishable (Tukey's HSD). Activated bleaching earths operate mainly through van der Waals interaction and cation exchange at porous surfaces that preferentially adsorb chromophoric pigments such as carotenoids and chlorophyll rather than free fatty acids;

Table 1: Mass and yield of oil at various bleaching earth doses.

Sample	Initial mass (g)	BE dose (%w/w)	BE mass (g)	Temp. (°C)	Time (min)	Final mass (g)	Yield (%)
M0 (control)	200.0	0	0.0	–	–	200.0	100.00
S1	200.0	1	2.0	80	30	199.2	99.60
S2	200.0	2	4.0	80	30	198.4	99.20
S3	200.0	3	6.0	80	30	197.6	98.80

Table 2: Oil quality parameters at various bleaching earth doses.

Parameter	M0 (control)	S1	S2	S3	Method
FFA (%)	7.22 ± 0.10	5.98 ± 0.10	5.98 ± 0.10	5.60 ± 0.10	Acid-base titration
Acid value (mg KOH/g)	14.36 ± 0.23	11.89 ± 0.19	11.90 ± 0.20	11.14 ± 0.20	Calculated from FFA

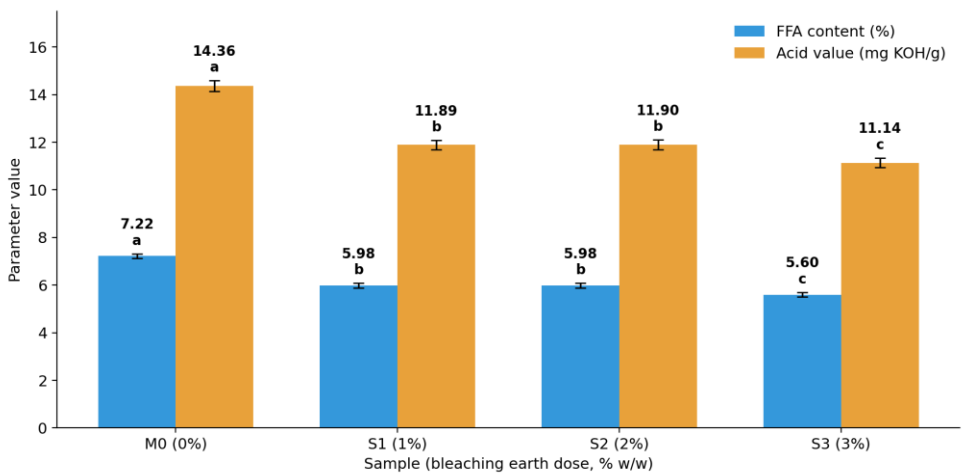


Figure 2: Reduction of FFA content (%) and acid value (mg KOH/g) at various bleaching earth doses. Bars show mean ± SD (n = 3); within each parameter, means that do not share a letter differ significantly (Tukey's HSD, $p < 0.05$; FFA: $F = 149.71$; acid value: $F = 140.01$).

once these high-affinity sites saturate, additional adsorbent contributes only low-affinity capacity that is largely ineffective for FFA removal [34]. Because the resulting FFA level remained well above the < 1.0% threshold generally required for base-catalyzed transesterification, an acid-catalyzed esterification pretreatment was mechanistically unavoidable rather than merely optional, a point often left implicit in WCO-PCM studies that bypass refining altogether.

3.2 *Acid-catalyzed esterification*

FFA decreased progressively with catalyst dose, reaching 0.55 ± 0.09% at 4.0 g H_2SO_4 (S6), a 92.4% reduction relative to untreated oil and 90.2% relative to the bleached feedstock. One-way ANOVA confirmed a highly significant effect of catalyst dose ($F = 2735.69 > F_{crit} = 4.07$; p-value < 0.0001), and Tukey's HSD placed S6 in a distinct group from both S4 and S5. Mechanistically, H_2SO_4 protonates the carbonyl oxygen of the free fatty acid, raising its electrophilicity and enabling nucleophilic attack by methanol to form methyl esters and water [32]; homogeneous acid pretreatment remains the most robust route for feedstocks in this FFA band, whereas ion-exchange and bifunctional heterogeneous systems trade simplicity for reusability [35], [29]. Comparable two-step acid–base schemes have lowered FFA sufficiently for alkaline transesterification of high-FFA crude palm kernel oil [11], and response surface and process-simulation studies of palm-derived biodiesel identify the methanol-to-oil ratio and catalyst loading as the dominant variables [12]. The catalyst-dose screening used here is a one-factor version of that approach; a full response-surface optimization is planned for scale-up.

Oil recovery rose in parallel with catalyst dose (92.55%, 93.20%, 93.85%), consistent with more complete FFA conversion reducing emulsion formation and oil entrainment in the aqueous-methanol phase (Table 3). Kinematic viscosity fell from 56.12 to 50.07 cSt, a 10.8% decrease (Figure 3a) attributable to conversion of carboxyl-bearing FFA, which dimerizes through intermolecular hydrogen bonding, into methyl esters that lack this association. Density decreased from 0.940 to 0.898 g/cm³, placing S6 within the range reported for pure FAME (0.86–0.90 g/cm³) (Figure 3b), while absorbance at 470 nm dropped from 0.721 to 0.148, reflecting removal of residual pigments during the methanol wash (Table 4 and Figure 4). S6 was therefore selected as the optimum esterification condition.

Table 3: Mass and yield of oil at various H_2SO_4 catalyst doses.

Sample	Initial mass (g)	H_2SO_4 (g)	Methanol (g)	Temp. (°C)	Time (min)	Final mass (g)	Yield (%)
M0 (control)	200.0	0.0	–	–	–	200.0	100.00
S4	200.0	2.0	45.0	60	60	185.1	92.55
S5	200.0	3.0	45.0	60	60	186.4	93.20
S6	200.0	4.0	45.0	60	60	187.7	93.85

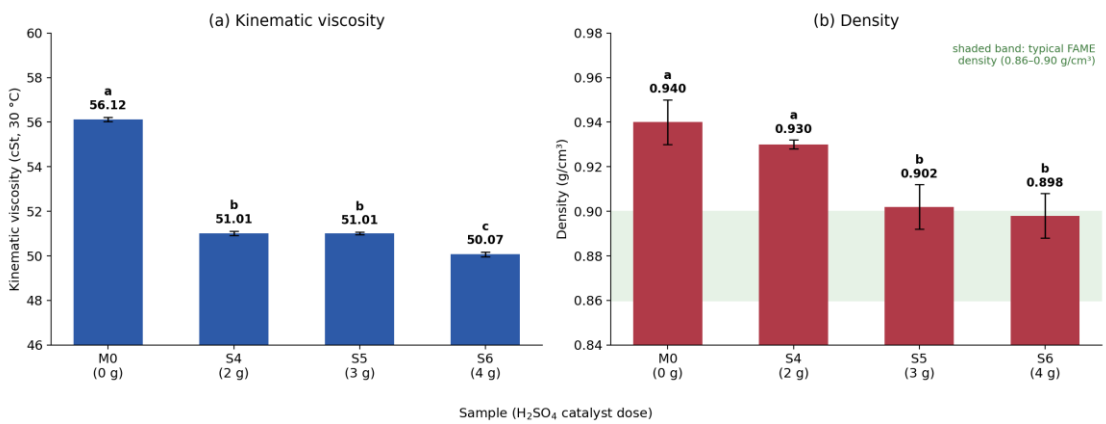


Figure 3: (a) Kinematic viscosity and (b) density of the oil after acid esterification at various H_2SO_4 doses. Bars show mean ± SD (n = 3); means that do not share a letter differ significantly (Tukey's HSD, p-value < 0.05; viscosity: F = 2787.50; density: F = 16.88).

Table 4: Oil quality parameters at various H_2SO_4 doses.

Parameter	M0	S4	S5	S6	Method
FFA (%)	7.22 ± 0.10	1.64 ± 0.06	1.26 ± 0.14	0.55 ± 0.09	Titration
Acid value (mg KOH/g)	14.36 ± 0.23	3.25 ± 0.11	2.51 ± 0.28	1.08 ± 0.17	Calculated
Viscosity (cSt, 30 °C)	56.12 ± 0.10	51.01 ± 0.10	51.01 ± 0.05	50.07 ± 0.10	Ostwald viscometer
Density (g/cm³)	0.940 ± 0.01	0.930 ± 0.002	0.902 ± 0.01	0.898 ± 0.01	Pycnometer
Absorbance (470 nm)	0.721 ± 0.007	0.186 ± 0.012	0.159 ± 0.005	0.148 ± 0.009	Colorimeter

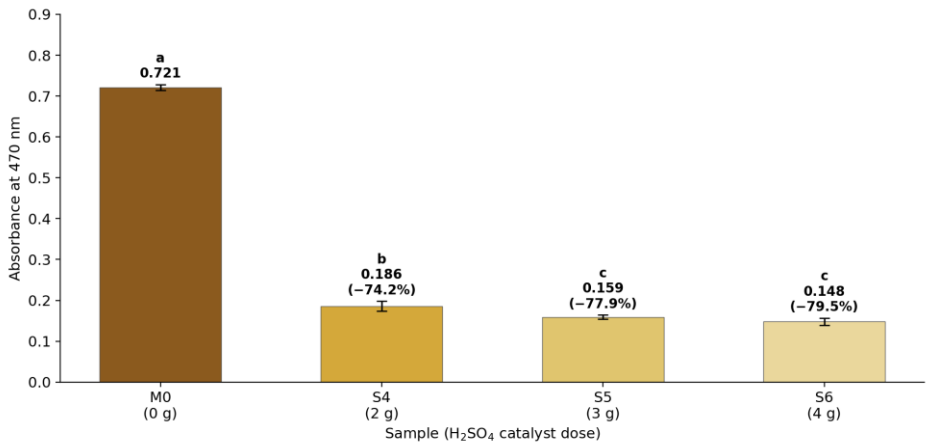


Figure 4: Oil colour, expressed as absorbance at 470 nm, after bleaching and esterification. Bars show mean ± SD (n = 3); means that do not share a letter differ significantly (Tukey's HSD, *p*-value < 0.05; F = 3119.37). Percentages give the reduction relative to the untreated oil (M0).

Table 5: FAME quality after base-catalyzed transesterification (triplicate).

Parameter	Method	Rep. 1	Rep. 2	Rep. 3	Mean ± SD
Yield (% mass)	Gravimetric	94.8	93.6	95.4	94.60 ± 0.92
Ester content (%)	EN 14103 / ^{1}H-NMR	97.8	96.9	97.9	97.53 ± 0.55
Acid value (mg KOH/g)	AOCS Cd 3d-63	0.28	0.33	0.25	0.29 ± 0.04
Viscosity (cSt, 40 °C)	ASTM D445	4.32	4.18	4.45	4.32 ± 0.14
Density (g/mL, 40 °C)	ASTM D1480	0.87	0.86	0.88	0.87 ± 0.01
Glycerol by-product (g)	Gravimetric	26.4	24.8	28.1	26.4 ± 1.7

3.3 *Base-catalyzed transesterification*

Transesterification of S6 gave a mean FAME yield of 94.60 ± 0.92% (160.8 g from 170.0 g oil) and an ester content of 97.53 ± 0.55%, exceeding the 96.5% minimum of EN 14214 and SNI 7182. The high yield and purity confirm that lowering FFA below 1.0% suppressed saponification, which otherwise compromises yield and complicates phase separation when FFA-rich feedstocks are transesterified with homogeneous alkaline catalysts [7], [35]. All three replicates met the EN 14214/SNI 7182 minimum, with the closest (96.9%) still 0.4 percentage points clear of the threshold, demonstrating reliable process performance. The density of the FAME, measured at 40 °C according to ASTM D1480, was 0.87 ± 0.01 g/mL (Table 5). Because biodiesel density rises by only about 0.02 g/mL on cooling from 40 to 15 °C, this value is consistent with the EN 14214 range of 0.860–0.900 g/mL at 15 °C and with the range typically reported for biodiesel from common feedstocks [36]. It is also lower than the 0.898 g/cm³

measured for the esterified oil (Table 4), as expected when triglycerides are converted to methyl esters. FAME of this quality is suitable as the base fuel for blending studies such as recent engine tests of ternary blends based on WCO biodiesel [13].

Acid value fell to 0.29 ± 0.04 mg KOH/g, 57% of the EN 14214 maximum, and kinematic viscosity dropped to 4.32 ± 0.14 cSt at 40 °C, more than a twelve-fold reduction relative to crude oil, consistent with near-complete conversion of triglycerides to methyl esters (Figure 5). A mass balance across the reaction (201.7 g total reactants: 170.0 g oil, 30.0 g methanol, 1.7 g KOH) accounted for 187.2 g (92.8%) of measurable product, comprising 160.8 g FAME and 26.4 ± 1.7 g crude glycerol, giving a FAME-to-crude-glycerol mass ratio of approximately 6.1:1. Based on the GC-MS mean ester molar mass (≈ 247 g/mol, corresponding to a triglyceride molar mass of ≈ 738 g/mol) and correcting for the 5.60% FFA already converted during esterification, the stoichiometric glycerol yield is ≈ 20.0 g (≈ 11.8% w/w of oil), equivalent to a stoichiometric FAME-to-glycerol mass ratio of ≈ 8.1:1. The measured crude glycerol mass (26.4 g, 15.55% w/w) therefore exceeds the theoretical value by ≈ 6.4 g, implying a glycerol content of roughly 76% in the crude phase. The excess is attributed to unreacted methanol (≈ 35% stoichiometric excess, which partitions preferentially

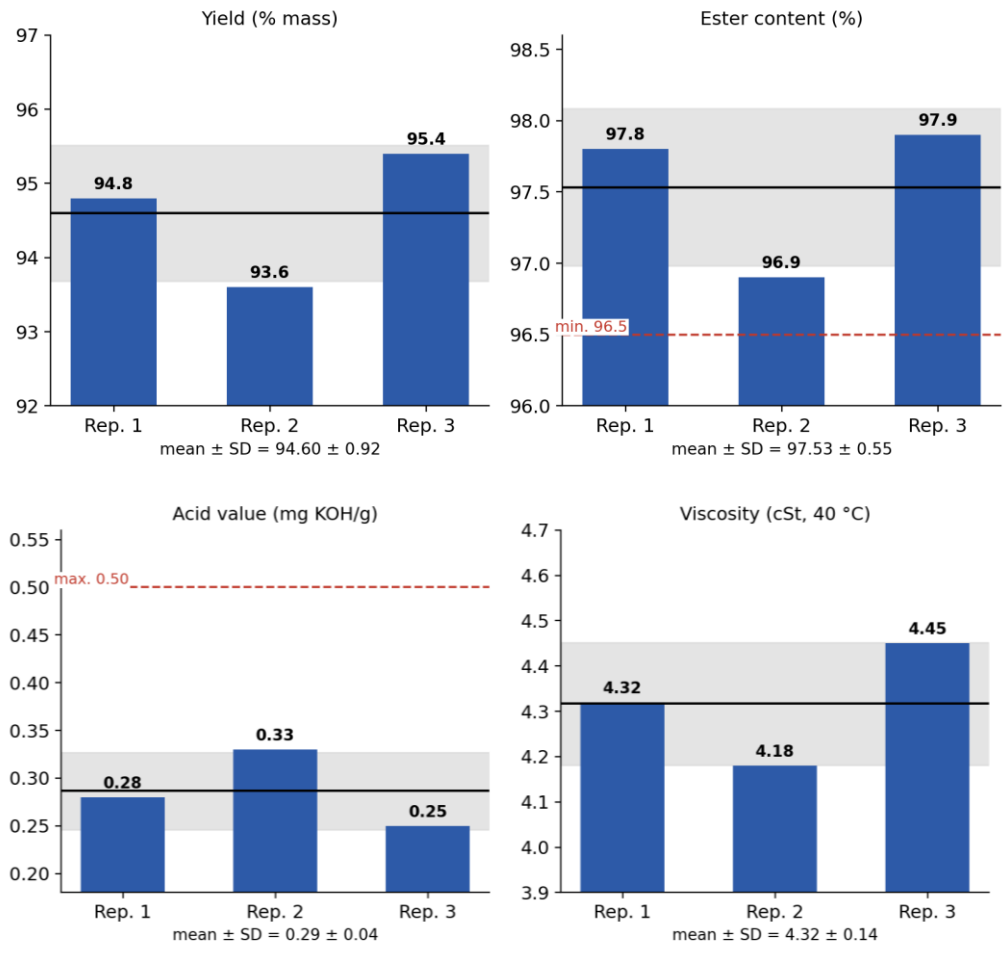


Figure 5: FAME quality parameters from triplicate transesterification runs relative to EN 14214 / SNI 7182:2015 thresholds. Bars: individual replicates; solid line: mean; grey band: ± 1 SD (n = 3); dashed line: standard threshold. Tukey letters are not shown because a single process condition was replicated.

into the glycerol phase), dissolved KOH and potassium methoxide, potassium soaps formed from residual FFA, and entrained FAME. Crude glycerol purities of 15–83% are typical of alkali-catalyzed biodiesel from waste oils [37], so the value obtained here is within the expected range, and the crude phase is suitable for downstream valorization, for example, acetylation to fuel additives [15]. The remaining ≈ 7.2% loss is attributed to methanol evaporation, dissolution of polar impurities into the wash water, and mechanical handling losses.

3.4 *Winterization and Bio-PCM isolation*

Cooling to 10–12 °C without agitation yielded a solid, saturated-rich fraction at 33.22 ± 2.41% of total FAME mass, with the balance retained as a liquid, unsaturated-rich fraction (Table 6). In cold-flow practice, this same operation is performed to reject the solid so that cloud and pour point fall, and the crystallized mass is reported as a yield penalty of the fuel product [24], [25]. Reading the identical separation in the opposite direction, as the recovery step for a value-added thermal storage material, converts what is conventionally a 33% loss into a co-product, and is the central process contribution of this work. On the scale used here, 170 g of esterified WCO delivered approximately 107 g of liquid FAME (Fl) plus 53 g of Bio-PCM candidate (Fs). Because winterization removes only ester species and introduces no contaminants, the ester content of Fl is expected to remain above the EN 14214 minimum while its cold-flow properties improve; however, Fl itself was not tested in this study, so its compliance with EN 14214/ASTM D6751 (ester content, density, viscosity, acid value, cloud point and CFPP) remains to be confirmed before it is described as fuel-grade.

Liquid entrainment. The single cold-methanol wash removes liquid adhering to the outer surface of the filter cake but cannot be assumed to remove all entrained liquid. Two observations show that removal was incomplete. First, Fs still contained 22.5% unsaturated FAME, mainly methyl oleate (21.27%), which melts at ≈ −20 °C and should not crystallize at 10–12 °C; part of this material is therefore occluded mother liquor rather than co-crystallized ester. Second, the Fs yield varied by ± 2.41% between replicates, consistent with variable retention of liquid in the cake. Conversely, methanol dissolves a small proportion of the saturated esters, so more extensive washing trades purity for yield. Residual methanol was not evident in TGA: the blends lost less than 1% of their mass up to 100 °C (Section 3.6). Entrainment will be quantified from the iodine value of Fs before and after a second wash, and multi-stage washing or solvent-assisted crystallization [24], [25] is expected to reduce it.

Energy requirement of winterization. Cooling FAME from ≈ 30 °C (tropical ambient) to 11 °C requires ≈ 38 kJ/kg of sensible heat (cp ≈ 2.0 kJ/kg·K), plus the heat of crystallization of the solid fraction; taking the measured Fs yield (33%) and a conservative upper-bound latent heat of 150 J/g for the crystallized esters adds ≈ 50 kJ/kg, giving ≤ 90 kJ/kg of FAME. With a chiller coefficient of performance of about 3 and allowance for heat gains during the 24 h hold, the electrical demand is of the order of 0.01–0.05 kWh per kg of FAME (≈ 0.04–0.2 MJ/kg), less than 0.5% of the lower heating value of biodiesel (≈ 37 MJ/kg). The energy penalty is therefore small relative to the fuel value of Fl, and the step is economically justified if the ≈ 0.33 kg of Fs obtained per kg of FAME can be sold above the price of biodiesel; biorefinery analyses of WCO likewise show that co-products largely determine overall viability [14]. A full techno-economic assessment, including the lower energy-storage value of Fs relative to commercial PCMs (Section 3.6), is beyond the scope of this work.

Table 6: Yield of the Bio-PCM candidate fraction (Fs) from winterization.

Replicate	Total FAME F (g)	Frozen FAME Fs (g)	Residual FAME Fl (g)	Bio-PCM yield Fs/F (%)
1	161.16	52.40	108.76	32.51
2	159.12	49.70	109.42	31.23
3	162.18	58.20	103.98	35.89
Mean ± SD	160.82 ± 1.56	53.43 ± 4.34	107.39 ± 2.97	33.22 ± 2.41

3.5 *GC-MS composition and Bio-PCM suitability*

GC-MS confirmed that winterization enriched SFAME from 72.8% in the parent FAME to 76.8% in the solid fraction while depleting UFAME from 27.1% to 22.5%. The dominant components of Fs were methyl palmitate (C16:0, 29.23%), methyl oleate (C18:1, 21.27%), methyl laurate (C12:0, 21.22%), methyl myristate (C14:0, 11.06%), and methyl stearate (C18:0, 6.05%). Notably, methyl stearate was concentrated 2.5-fold (2.45% → 6.05%), the single largest relative enrichment in the fraction, identifying C18:0 as the primary nucleating species. Figure 6(a) shows the parent FAME (F) before winterization, i.e., the feed biodiesel labelled 'initial biodiesel' in the original chromatogram, and Figures 6(b) and 6(c) show the solid and liquid fractions; the major-component comparison is summarized in Figure 7.

Tables 7 and 8 report relative total-ion-current peak areas and are therefore semi-quantitative. A component mass balance using the measured Fs/F split (33.2%) reproduces the parent composition within 0.7 percentage points for methyl myristate and methyl oleate but deviates by 2–3 percentage points for methyl laurate, methyl palmitate and methyl stearate, which reflects differences in electron-ionization response factors and single-injection variability. Differences of this magnitude between F, Fs and Fl are therefore interpreted as trends, and quantitative confirmation by GC-FID with an internal standard (EN 14103) is in progress.

The non-FAME peaks eluting at 20–21 min (0.62% in Fs and 0.41% in Fl; below the detection threshold in F) were assigned to long-chain hydrocarbons by mass-spectral library matching. They most plausibly originate from thermal degradation during repeated deep frying, in which radical cleavage, decarboxylation and polymerization of acyl chains generate hydrocarbons, aldehydes, ketones and oligomers [38], [39], with a possible contribution from naturally occurring hydrocarbons (e.g., squalene) in the original oil or the fried food. Unreacted lipid structures are an unlikely source: residual mono-, di- and triacylglycerols are not volatile under the GC-MS conditions used, would not give hydrocarbon-type mass spectra, and are already limited by the 97.53% ester content (Table 5). Their slight concentration in Fs is consistent with the low solubility of long-chain saturated hydrocarbons in the cold ester phase, which causes them to co-precipitate with the saturated esters.

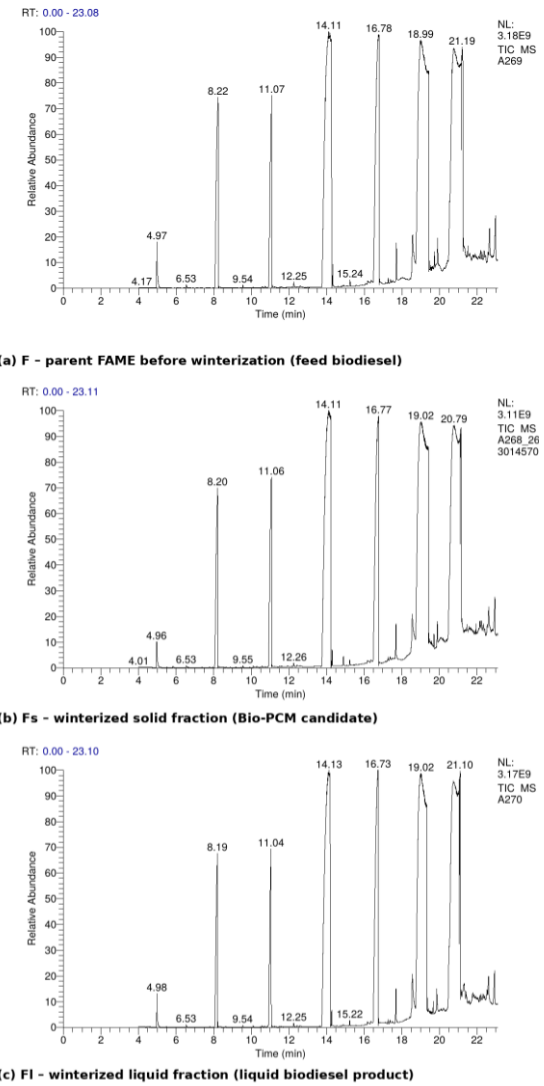


Figure 6: GC-MS total-ion chromatograms of (a) parent FAME before winterization (F; the feed biodiesel, termed 'initial biodiesel' in the original instrument report), (b) winterized solid fraction (Fs), and (c) residual liquid fraction (Fl).

The enrichment pattern is explained by component melting points: methyl stearate (≈ 37.7 °C), methyl palmitate (≈ 30.5 °C), and methyl myristate (≈ 18.5 °C) melt at or above the winterization temperature and nucleate readily as cooling proceeds, whereas the cis double bond of methyl oleate (≈ –19.9 °C) introduces a molecular kink that obstructs crystal-lattice packing [22], keeping it preferentially in Fl. The apparent anomaly

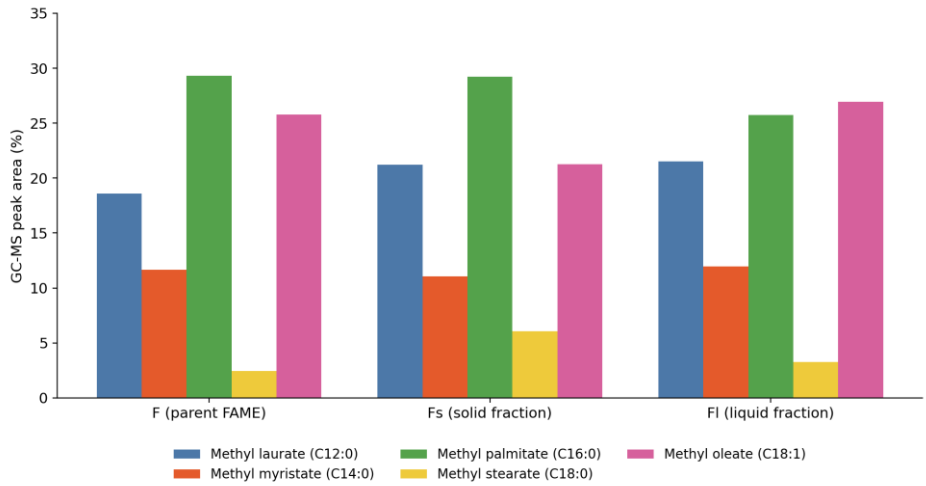


Figure 7: Comparison of the major FAME components (% GC-MS peak area) among F, Fs, and Fl.

Table 7: Fatty acid methyl ester composition of F, Fs, and Fl by GC-MS.

RT (min)	Compound	Class	F (%)	Fs (%)	Fl (%)
~5.0	Methyl hexanoate (C6:0)	Saturated	0.37	0.23	0.26
~8.2	Methyl octanoate (C8:0)	Saturated	4.84	4.11	3.93
~11.0	Methyl decanoate (C10:0)	Saturated	4.43	4.02	3.76
~14.1	Methyl laurate (C12:0)	Saturated	18.58	21.22	21.51
~16.7	Methyl myristate (C14:0)	Saturated	11.68	11.06	11.95
~17.7	Methyl pentadecanoate (C15:0)	Saturated	0.38	0.38	0.29
~18.6	Methyl palmitoleate (C16:1)	Unsaturated	0.67	0.64	0.78
~19.0	Methyl palmitate (C16:0)	Saturated	29.32	29.23	25.76
~20.8	Methyl oleate (C18:1)	Unsaturated	25.77	21.27	26.93
~21.1	Methyl stearate (C18:0)	Saturated	2.45	6.05	3.27
~22.6	Methyl cis-eicosenoate (C20:1)	Unsaturated	0.64	0.63	0.40
~22.9	Methyl eicosanoate (C20:0)	Saturated	0.72	0.54	0.44
~20–21	Long-chain hydrocarbons (non-FAME)	Impurity	–	0.62	0.41

Table 8: Classification of saturated and unsaturated FAME content.

Sample	SFAME (%)	UFAME (%)	Impurity (%)
F (parent FAME/biodiesel)	72.8	27.1	~0
Fs (frozen fraction)	76.8	22.5	0.6
Fl (residual liquid fraction)	71.2	28.1	0.4

is methyl laurate, which melts at ≈ 5.2 °C yet appears at a slightly higher proportion in Fs (21.22%) than in F (18.58%) (Tables 7 and 8, Figure 7). Because Fl shows a similar value (21.51%), this difference is close to the analytical uncertainty noted above; where it is real, it is tentatively attributed to co-crystallization, in which the lattice formed by the long-chain saturated esters co-crystallizes shorter-chain

saturated esters that would remain liquid in isolation. The same mechanism accounts for the modest overall SFAME enrichment (4.0 percentage points) achieved in a single stage: co-crystallization inevitably carries some unsaturated material into the solid, so multi-stage or solvent-assisted fractionation would be required for sharper separation.

Because Fs is a multi-component mixture rather than a pure compound, its solid–liquid transition is expected to occur over a melting range governed by eutectic interaction among its dominant C12–C18 saturated esters. With methyl palmitate as the principal component and eutectic contributions from methyl laurate, methyl myristate, and methyl stearate, the expected range falls within approximately 20–30 °C, the window relevant to indoor thermal comfort and to reported methyl-ester and fatty-acid eutectic Bio-PCM [22], [23]. This positions Fs favourably against paraffin systems on renewability and cost grounds [1], [40]-[42], although not yet on energy-storage density (Section 3.6). The 20–30 °C range estimated above reflects a compositional inference from constituent melting points. Section 3.6 reports the measured DSC and TGA behaviour of Fs–stearic acid eutectic blends. Blends containing 15–25 wt% stearic acid melted between about 29 and 48 °C, above the 20–30 °C range inferred from composition, and lost little mass below 100 °C. The Fs–stearic acid system is therefore a candidate for encapsulation into building panels only once the latent-heat limitation discussed in Section 3.6 is addressed [27], [28], [29].

3.6 *Differential scanning calorimetry and thermogravimetric analysis of Bio-PCM eutectic formulations*

To evaluate Fs as a Bio-PCM near its service temperature, five eutectic formulations were prepared by blending 5 g of Fs with stearic acid at 5, 10, 15, 20, and 25 wt% of the total blend mass (P1–P5, respectively) and characterized by DSC and TGA as described in Section 2.7. Air was used for the DSC survey of P1–P5 because it is the service laboratory's default purge for routine DSC, whereas TGA was run under nitrogen so that evaporation of the esters could be distinguished from oxidative decomposition. All DSC runs used sealed pans, so the sample was exposed only to the small volume of gas trapped in the pan, and in air the first oxidative exotherm appeared only above about 135 °C, well after melting was complete. Oxidation was therefore not expected to affect the melting endotherm. To verify this, P3 and P5 were also analysed under nitrogen (Table 10, Figure 9).

No quantifiable solid–liquid transition was detected for P1, indicating that 5 wt% stearic acid is insufficient to nucleate a coherent crystalline phase under these scan conditions. P2 showed only a weak transition (0.89 J/g) at 24.04–28.10 °C, within the nominal 20–30 °C comfort band but too small in magnitude for practical thermal storage. Because data were recorded from about 20 °C, this transition lies inside the measured range and is not a start-up artefact. P3, P4, and P5 each showed a well-defined transition (Table 9, Figure 8), together with a second, smaller exothermic event at approximately 135–197 °C that is attributed to thermal oxidation under the air atmosphere used for this test rather than to a solid–liquid phase change, and is therefore excluded from the Bio-PCM evaluation. Onset temperature did not increase monotonically with stearic acid content (P3, 36.07 °C exceeding P4, 31.46 °C), a pattern consistent with the non-ideal, multicomponent eutectic behaviour expected of a mixture this compositionally complex rather than with measurement error.

Measurements under nitrogen. Table 10 and Figure 9 compare the air and nitrogen data for P3 and P5. Under nitrogen, both blends showed a single melting endotherm, at lower temperatures and with much smaller enthalpy than under air: the peak of P3 moved from 38.18 to 32.26 °C and its ΔH fell from 11.62 to 1.67 J/g, while the peak of P5 moved from 43.18 to 34.20 °C and its ΔH fell from 28.08 to 8.08 J/g. Re-integration of the exported raw data reproduced the instrument values (1.70 and 8.08 J/g). No exothermic event or baseline drift attributable to oxidation was seen in either atmosphere below 80 °C.

Comparison of the air and nitrogen data. The 70–86% lower ΔH under nitrogen is far larger than oxidation can explain. All runs used sealed pans, the samples spent only a few minutes above 30 °C, and saturated methyl esters, which dominate Fs, are the most oxidation-resistant biodiesel components. Three other factors are more likely. First, the blends are not homogeneous solids: at room temperature they consist of stearic-acid-rich crystals dispersed in liquid esters, and the solid settles, as was also seen during winterization. Aliquots of 2–5 mg taken from such a material can therefore contain quite different amounts of crystalline phase. Second, the nitrogen runs were made on samples that had been stored about six weeks longer at room temperature (Figure 1i), with partial

Table 9: DSC transition parameters of Fs–stearic acid eutectic formulations (P1–P5) under air (sealed pans, 10 °C/min).

Sample	Stearic acid (wt%)	Mass (mg)	Onset (°C)	Peak (°C)	Endset (°C)	ΔH (J/g)
P1	5	2.780	–	–	–	n.d.*
P2	10	2.960	24.04	26.60	28.10	0.89
P3	15	3.880	36.07	38.18	42.05	11.62
P4	20	3.640	31.46	36.90	42.11	10.55
P5	25	2.450	32.96	43.18	48.39	28.08

*n.d. = no quantifiable transition detected.

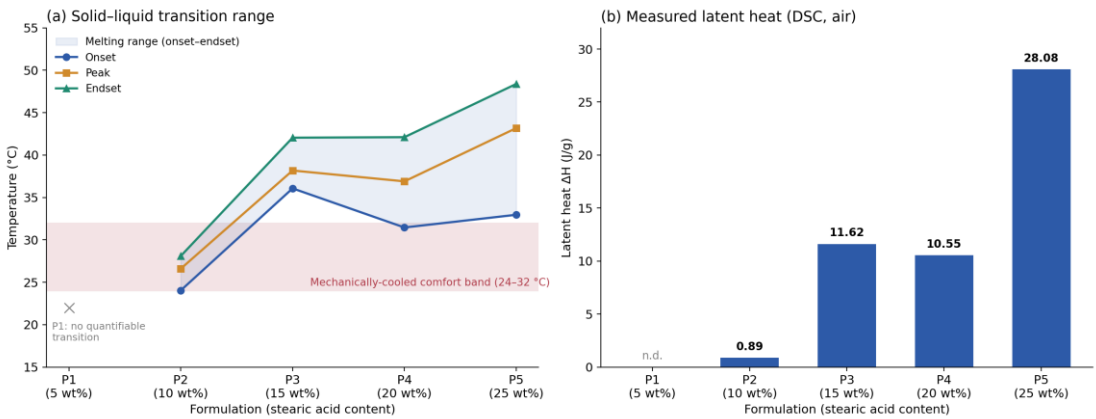


Figure 8: DSC characterization of Fs–stearic acid eutectic formulations P1–P5: (a) solid–liquid transition range (onset, peak, endset) versus stearic acid content, with the mechanically-cooled comfort band (24–32 °C) shaded; (b) measured latent heat (ΔH) by formulation.

melting and refreezing every day, which can segregate the phases and change the crystal form of stearic acid; polymorphic transformation during storage is well known to alter the melting temperature and enthalpy of fats and fatty acids [43]. Third, the integration baseline is less certain for the air runs, because recording started at about 20 °C and the endotherm followed the start-up transient closely; under nitrogen, the scan started at 10 °C, and the melting peak sat on a stable baseline. Melting enthalpies of PCMs are known to depend on sample preparation, sample mass, baseline construction and measurement mode, and inter-laboratory comparisons have reported large spreads for the same material [44], [45]. Here, too, the integrated value is sensitive to the baseline: widening the integration window of the nitrogen run of P5 from 29.7–40.1 °C to 26–42 °C raises ΔH from 8.1 to 15.5 J/g. The nitrogen values are therefore taken as the conservative reference in this work, and the air values as an upper bound. The ranking is the same under both gases: P5 stored more heat than P3. Replicate measurements on freshly homogenized samples, with heat–cool–heat programmes, are needed before a design value of ΔH can be given.

Thermogravimetric behaviour and choice of working formulation. P3 and P4 lost 0.94% and 0.42% of their mass up to 100 °C, respectively, so neither blend evaporates appreciably in the 35–45 °C range expected on a sun-exposed envelope. At higher temperatures, the two curves diverge: P3 retained 97.49% of its mass at 300 °C and P4 only 78.34%, most of the loss of P4 occurring above 200 °C. The instrument files show that the two runs used different pan closures (crimped for P3, sealed for P4) and that the atmosphere field of the P3 file reads air, so this difference cannot be attributed to the formulation and is not used to rank the blends. P5 was not analysed by TGA. Latent heat is the property that limits this material, and P5 gave the highest value under both air and nitrogen; P5 (25 wt% stearic acid) is therefore carried forward as the working formulation, while P3 and P4, which melt in a similar window, are kept as alternatives.

Latent heat limitation. Even the best value measured here (P5: 8.08 J/g under nitrogen, 28.08 J/g in air) is one to two orders of magnitude below that of benchmark PCMs. Fatty-acid eutectics typically store 127–205 J/g [20], [21], pure methyl palmitate and

Applied Science and Engineering Progress, Vol. 20, No. 4, 2027, 8390

Table 10: DSC melting parameters of P3 and P5 under air and nitrogen; sealed aluminium pans, 10 °C/min.

Sample	Purge gas	Mass (mg)	Onset (°C)	Peak (°C)	Endset (°C)	ΔH (J/g)
P3	Air	3.880	36.07	38.18	42.05	11.62
P3	N_2	4.510	29.27	32.26	36.89	1.67
P5	Air	2.450	32.96	43.18	48.39	28.08
P5	N_2	4.820	31.00	34.20	38.98	8.08

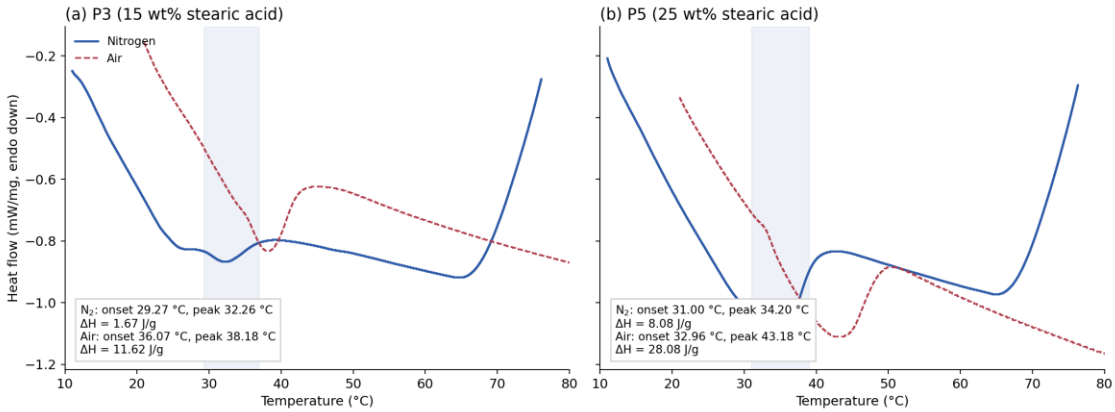


Figure 9: DSC heating curves of (a) P3 and (b) P5 under nitrogen (solid lines) and air (dashed lines), normalized by sample mass. The shaded band marks the onset–endset range under nitrogen. The rise above about 65 °C in the nitrogen runs is the instrument approaching the 80 °C isothermal hold.

methyl stearate store about 200 J/g [22], and commercial paraffin and bio-based PCMs store 150–250 J/g [2], [3]. In practical terms, a 10 mm layer of P5 (≈ 8.7 kg/m² at ≈ 870 kg/m³) would store only about 0.07 MJ/m² per melting cycle under nitrogen (0.24 MJ/m² at the air value), against about 1.6 MJ/m² for the same thickness of a 180 J/g PCM, which is impractical for gypsum or cementitious panels. The blends are therefore reported as proof-of-concept Bio-PCM candidates from a waste stream, not as high-performance PCMs. Two features of the system explain the low latent heat. First, the C6–C14 esters (≈ 41% of Fs) and the unsaturated esters (≈ 22%) are liquid above 30 °C, so about 63% of Fs acts as a solvent that dilutes the crystallizable fraction. Second, the transition temperature and ΔH rose with stearic acid content, which indicates that the endotherm is dominated by the melting and dissolution of stearic-acid-rich crystals in the ester matrix (liquidus behaviour) rather than by a true eutectic of all components. The nitrogen runs, which began at 10 °C, showed only a broad sloping signal below the main peak that could not be separated from the start-up transient, so little additional latent heat appears to be hidden at lower temperatures. In order of expected impact, the latent heat could be raised by (i) multi-stage crystallization at progressively higher temperatures, which concentrates methyl palmitate and methyl stearate and rejects short-chain and unsaturated esters [24], [25]; (ii) solvent-assisted fractionation, for example in methanol or acetone, which reduces liquid occlusion and raises the saturated FAME purity of the solid [25]; (iii) raising the fatty-acid fraction above 25 wt%, or replacing stearic acid with lauric, myristic or palmitic acid to form true binary or ternary eutectics with methyl palmitate, which store more than 150 J/g [22], [20]; and (iv) shape-stabilization or microencapsulation, which does not raise ΔH but prevents leakage of the liquid ester fraction [28], [30]. These routes are being evaluated in the second stage of this programme.

Target building application. Under nitrogen, P5 melted between 31.00 and 38.98 °C (peak 34.20 °C), above the 20–30 °C indoor comfort band [16], [17], so it is not intended for interior wallboards. It is intended for exterior building envelopes, namely roof layers beneath tiles or metal sheeting and sun-exposed wall panels, where surface temperatures in tropical climates regularly reach 35–45 °C at peak solar irradiance and fall below 30 °C at night, allowing the material to melt and resolidify every day [19], [18]. In this position, the PCM intercepts part of the solar heat gain before it reaches the interior; organic PCMs

melting at 35–37 °C have reduced roof cooling loads in hot climates [19], and roof-integrated PCM has been more effective than wall-integrated PCM under tropical conditions [17].

Re-evaluation of P2 and tuning toward the comfort band. P2 (onset 24.04 °C, peak 26.60 °C, endset 28.10 °C) is the only formulation whose transition lies within the indoor comfort band [16], [17], but its latent heat (0.89 J/g) is negligible, which suggests that at 10 wt% almost all of the stearic acid stays dissolved in the liquid esters. P2 is therefore kept as the starting point for indoor formulations rather than discarded. The transition of Fs-based blends can be moved downward while keeping or raising ΔH by (i) replacing stearic acid with a lower-melting fatty acid (lauric, capric or myristic acid), because the liquidus of a binary system falls with the melting point of its higher-melting component; (ii) formulating toward the eutectic of methyl palmitate with a C10–C12 fatty acid, which melts at about 20–26 °C with high latent heat [22], [20], [21]; and (iii) using a more saturated, palmitate-rich Fs from multi-stage fractionation so that the ester itself contributes latent heat. A composition series at 7–13 wt% stearic acid and blends containing palmitic acid are included in the next stage of this work.

Thermal reliability. Quantitative thermal-cycling data are not yet available. The observation that the blends solidified overnight and melted during the day in an unconditioned room is qualitative and does not replace accelerated testing. Reliability testing over at least 300–1000 DSC heating–cooling cycles, the range recommended to represent one to several years of daily service [20], [21], with onset temperature and ΔH compared before and after cycling and FTIR used to detect chemical change, is part of the ongoing microencapsulation study and will be reported with the encapsulated material [46], [47].

4 Conclusions

This study showed that one WCO batch can yield both biodiesel and a solid Bio-PCM candidate when winterization is run as a co-production step instead of a cold-flow correction. The main findings are as follows. (1) Bleaching with 3% activated bleaching earth removed pigments but lowered FFA only from 7.22% to 5.60%, so acid esterification was necessary; 4.0 g H_2SO_4 reduced FFA to 0.55 ± 0.09% (p-value < 0.0001). (2) KOH-catalyzed transesterification gave a FAME yield of 94.60 ± 0.92% and an ester content of 97.53 ± 0.55%, meeting EN 14214 and SNI 7182; the mass balance closed to 92.8%, and the excess crude-glycerol mass was explained by retained methanol, catalyst and soap. (3) A single cooling stage at 10–12 °C isolated 33.22 ± 2.41% of the FAME as a solid fraction enriched in saturated esters (72.8% to 76.8%) and dominated by methyl palmitate, methyl laurate and methyl myristate; 170 g of esterified oil gave about 107 g of liquid FAME and 53 g of Bio-PCM candidate. (4) In five Fs–stearic acid blends, transition temperature and latent heat rose with stearic acid content. Under nitrogen, the 25 wt% blend (P5) melted at 31.0–39.0 °C, which suits exterior envelopes such as roofs and sun-exposed walls; the 10 wt% blend (P2) melted within the comfort band (24–28 °C) but stored almost no heat. (5) Latent heats measured under nitrogen (1.67 J/g for P3 and 8.08 J/g for P5) were 70–86% lower than the values measured under air (11.62 and 28.08 J/g). The gap is attributed mainly to sample heterogeneity, storage and baseline definition rather than to oxidation. On either basis, the latent heat is far below that of commercial PCMs and is the main limitation of the material at its present stage. Future work will address multi-stage and solvent-assisted fractionation and eutectic formulation to raise the latent heat, replicate DSC with heat–cool–heat programmes on freshly homogenized samples, accelerated thermal-cycling tests, verification of the liquid fraction against fuel standards, and microencapsulation of the optimized formulation for building panels.

Acknowledgments

The authors would like to express their sincere gratitude to the Directorate of Research and Community Service, Directorate General of Research and Development, Ministry of Higher Education, Science, and Technology of the Republic of Indonesia, together with the Center for Research and Community Service (P3M) Politeknik Negeri Sriwijaya, for funding this research under the Fundamental Research Grant scheme for fiscal year 2026. Special thanks are also extended to the Chemical Engineering Laboratory at Politeknik Negeri Sriwijaya for providing laboratory facilities, and the Integrated Research and Testing Laboratory (LPPT), Universitas Gadjah Mada, for support in thermal analysis.

Author Contributions

A.Z.: conceptualization, project coordination, literature review, monitoring and evaluation, manuscript writing, and management of research outputs; M.A.: extraction and esterification/transesterification experiments, winterization fractionation, and interfacial synthesis optimization; R.D.: sample preparation, prototype development, and thermal performance testing; I.R.S.: laboratory characterization, GC-MS data analysis, and validation. All authors have read and agreed to the published version of the manuscript.

Conflicts of Interest

The authors declare no conflict of interest.

Declaration of generative AI and AI-assisted technologies in the writing process

The authors used a generative AI assistant solely for language editing and reference formatting. No content, data, analysis, or interpretation was generated by AI. The authors reviewed and verified all text and references and take full responsibility for the content of the manuscript.

References

[1] M. H. Jahangir and R. Alimohamadi, "A comparative evaluation on energy consumption of a building using bio-based and paraffin-based phase change materials integrated to external building envelope," *Energy Reports*, vol. 11, pp. 3914–3930, Jun. 2024, doi: 10.1016/j.egyr.2024.03.041.

[2] B. T. Nalla et al., "Bio-based phase-change materials for thermal energy storage: Recent advances, challenges, and outlook," *Results in Engineering*, vol. 28, 2025, Art. no. 107087, doi: 10.1016/j.rineng.2025.107087.

[3] M. Zadshir, B. W. Kim, and H. Yin, "Bio-based phase change materials for sustainable development," *Materials*, vol. 17, no. 19, 2024, Art. no. 4816, doi: 10.3390/ma17194816.

[4] H. Chu et al., "Advances in resource utilization of waste in phase change materials," *Journal of Energy Storage*, vol. 99, Oct. 2024, Art. no. 113342, doi: 10.1016/j.est.2024.113342.

[5] Z. Arman et al., "Green form-stable biocomposite of biochar from tea industry waste and organic phase change material," *Journal of Energy Storage*, vol. 101, 2024, Art. no. 113815, doi: 10.1016/j.est.2024.113815.

[6] W.-Y. Wu et al., "Advancements in sustainable phase change materials: Valorizing waste for eco-friendly applications," *Materials Today Chemistry*, vol. 39, 2024, Art. no. 102163, doi: 10.1016/j.mtchem.2024.102163.

[7] I. ul Haq et al., "Comparative analysis of various waste cooking oils for esterification and transesterification processes to produce biodiesel," *Green Chemistry Letters and Reviews*, vol. 14, no. 3, pp. 462–473, Jun. 2021, doi: 10.1080/17518253.2021.1941305.

[8] D. Chen et al., "Waste cooking oil applicable phase change capsules to improve thermoregulation of foamed concrete," *Construction and Building Materials*, vol. 432, 2024, Art. no. 136538, doi: 10.1016/j.conbuildmat.2024.136538.

[9] S. Hasbi, K. Y. Leong, K. Z. Ku Ahmad, N. Abdul Rahim, and M. S. Saharudin, "Development of coconut oil/capric acid eutectic phase change material with graphene as latent thermal energy storage," *International Journal of Automotive and Mechanical Engineering*, vol. 20, no. 1, pp. 10247–10257, Mar. 2023, doi: 10.15282/ijame.20.1.2023.07.0792.

[10] X. Wang et al., "Fatty acid from recycled waste cooking oil as a phase-change material for thermal storage systems," *RSC Advances*, vol. 16, no. 7, pp. 5852–5863, Feb. 2026, doi: 10.1039/D5RA07469J.

[11] E. Kurniasih, R. Rahmi, M. D. Supardan, and D. Darusman, "Two-step reaction for biodiesel synthesized from a high-free fatty acid crude palm kernel oil," *Applied Science and Engineering Progress*, vol. 18, no. 2, 2025, Art. no. 7570, doi: 10.14416/j.asep.2024.09.009.

[12] B. Dharmalingam, T. Phusantisampan, B. Paramasivam, and B. Saha, "Process modelling and optimization of palm oil biodiesel production using Aspen Plus and response surface methodology," *Applied Science and Engineering Progress*, vol. 19, no. 4, 2026, Art. no. 8235, doi: 10.14416/j.asep.2026.06.007.

[13] W. Roschat et al., "Performance enhancement of ternary blending of biodiesel, Yang-Na (Dipterocarpus alatus) oil, and plastic waste pyrolysis oil for agricultural diesel engines," *Applied Science and Engineering Progress*,

vol. 19, no. 4, 2026, Art. no. 8100, doi: 10.14416/j.asep.2026.03.003.

[14] J. R. H. Panjaitan, D. Y. Situmorang, and E. S. Tarigan, "Production and economic evaluation of biobased detergent from waste cooking oil," *Applied Science and Engineering Progress*, vol. 19, no. 4, 2026, Art. no. 8098, doi: 10.14416/j.asep.2026.04.002.

[15] H. Dewajani, L. C. Dewi, A. Mustain, R. D. Chrisnandari, and D. F. Akbar, "Dual-functionalized palm kernel shell biochar as a heterogeneous catalyst for glycerol acetylation toward biofuel additives," *Applied Science and Engineering Progress*, early access, 2026, Art. no. 8287, doi: 10.14416/j.asep.2026.08.013.

[16] K. Faraj, M. Khaled, J. Faraj, F. Hachem, and C. Castelain, "Phase change material thermal energy storage systems for cooling applications in buildings: A review," *Renewable and Sustainable Energy Reviews*, vol. 119, 2020, Art. no. 109579, doi: 10.1016/j.rser.2019.109579.

[17] M. Chen Austin, J. Araúz, and D. Mora, "Numerical assessment of different phase change materials as a passive strategy to reduce energy consumption in buildings under tropical climates," *Buildings*, vol. 12, no. 7, 2022, Art. no. 906, doi: 10.3390/buildings12070906.

[18] F. L. Rashid et al., "Recent advances and developments in phase change materials in high-temperature building envelopes: A review of solutions and challenges," *Buildings*, vol. 14, no. 6, 2024, Art. no. 1582, doi: 10.3390/buildings14061582.

[19] A. B. Huluka and S. Muthulingam, "Integrated spherical phase change modules in concrete roofs enhance thermal performance in hot climates," *Scientific Reports*, vol. 15, no. 1, 2025, Art. no. 39845, doi: 10.1038/s41598-025-23490-1.

[20] A. Anand et al., "A comprehensive review on eutectic phase change materials: Development, thermophysical properties, thermal stability, reliability, and applications," *Alexandria Engineering Journal*, vol. 112, pp. 254–280, Jan. 2025, doi: 10.1016/j.aej.2024.10.054.

[21] Z. Fan, Y. Zhao, X. Liu, Y. Shi, and D. Jiang, "Thermal properties and reliabilities of lauric acid-based binary eutectic fatty acid as a phase change material for building energy conservation," *ACS Omega*, vol. 7, no. 18, pp. 16097–16108, May 2022, doi: 10.1021/acsomega.2c01420.

[22] A. Alipour, F. Eslami, and S. M. Sadrameli, "A novel bio-based phase change material of methyl palmitate and decanoic acid eutectic mixture: Thermodynamic modeling and thermal performance," *Chemical Thermodynamics and Thermal Analysis*, vol. 10, 2023, Art. no. 100111, doi: 10.1016/j.ctta.2023.100111.

[23] K. Karthikeyan et al., "Preparation and thermal characterization of capric-myristic acid binary eutectic mixture with silver–antimony tin oxide and silver-graphane nanoplatelets hybrid-nanoparticles as phase change material for building applications," *Materials Letters*, vol. 328, 2022, Art. no. 133086, doi: 10.1016/j.matlet.2022.133086.

[24] H. Tajima, M. Abe, H. Komatsu, and K. Yamagiwa, "Feasibility of additive winterization of biodiesel fuel derived from various eatable oils and fat," *Fuel*, vol. 305, 2021, Art. no. 121479, doi: 10.1016/j.fuel.2021.121479.

[25] J. Liu and B. Tao, "Fractionation of fatty acid methyl esters via urea inclusion and its application to improve the low-temperature performance of biodiesel," *Biofuel Research Journal*, vol. 9, no. 2, pp. 1617–1629, Jun. 2022, doi: 10.18331/BRJ2022.9.2.3.

[26] A. Idouanaou et al., "Integrated evaluation of bio-based phase change materials to reduce operational and embodied carbon in service buildings across multiple climate zones," *Buildings*, vol. 15, no. 20, 2025, Art. no. 3720, doi: 10.3390/buildings15203720.

[27] H. Zhou, A. R. Puttige, G. Nair, and T. Olofsson, "Thermal behaviour of a gypsum board incorporated with phase change materials," *Journal of Building Engineering*, vol. 94, 2024, Art. no. 109928, doi: 10.1016/j.jobe.2024.109928.

[28] S. Nishad, P. Fajkus, M. Mrlík, D. Sanetrnik, and I. Krupa, "Composite panels utilizing TetraPak and microencapsulated phase change material for enhanced building thermal management," *Emergent Materials*, vol. 9, 2026, Art. no. 15, doi: 10.1007/s42247-026-01336-4.

[29] S. V. M. Ramasamy, V. Booramurthy, S. Pandian, M. D. Albaqami, and R. G. Alotabi, "Synthesis and characterization of magnetic bifunctional nano-catalyst for the production of

biodiesel from Madhuca indica oil," *Environmental Science and Pollution Research*, vol. 30, no. 25, pp. 66912–66922, May 2023, doi: 10.1007/s11356-023-26992-5.

[30] H. Paiva, F. Rebelo, A. Figueiredo, V. M. Ferreira, and R. Vicente, "Improving the incorporation of microencapsulated phase change materials into mortars through rheology-based analysis," *Materials and Structures*, vol. 59, 2026, Art. no. 111, doi: 10.1617/s11527-026-03004-9.

[31] Monika, S. Banga, and V. V. Pathak, "Biodiesel production from waste cooking oil: A comprehensive review on the application of heterogenous catalysts," *Energy Nexus*, vol. 10, 2023, Art. no. 100209, doi: 10.1016/j.nexus.2023.100209.

[32] M. Supeno, J. P. Sihotang, Y. V. Panjaitan, D. S. Y. Damanik, J. Br. Tarigan, and E. K. Sitepu, "Room temperature esterification of high-free fatty acid feedstock into biodiesel," *RSC Advances*, vol. 13, no. 47, pp. 33107–33113, Nov. 2023, doi: 10.1039/D3RA06912E.

[33] S. Machmudah et al., "Oil removal from spent bleaching earth of vegetable oil refinery plant using supercritical carbon dioxide," *Heliyon*, vol. 8, no. 10, 2022, Art. no. e10826, doi: 10.1016/j.heliyon.2022.e10826.

[34] E. Abedi et al., "Comparison between emerging and conventional methods for edible oils bleaching," *Food Science & Nutrition*, vol. 13, no. 11, 2025, Art. no. e71121, doi: 10.1002/fsn3.71121.

[35] S. Z. Abidin, M. L. Mohammed, and B. Saha, "Two-stage conversion of used cooking oil to biodiesel using ion exchange resins as catalysts," *Catalysts*, vol. 13, no. 8, 2023, Art. no. 1209, doi: 10.3390/catal13081209.

[36] S. K. Hoekman, A. Broch, C. Robbins, E. Ceniceros, and M. Natarajan, "Review of biodiesel composition, properties, and specifications," *Renewable and Sustainable Energy Reviews*, vol. 16, no. 1, pp. 143–169, Jan. 2012, doi: 10.1016/j.rser.2011.07.143.

[37] C. Decarpigny et al., "Bioprocesses for the biodiesel production from waste oils and valorization of glycerol," *Energies*, vol. 15, no. 9, 2022, Art. no. 3381, doi: 10.3390/en15093381.

[38] C. G. Lopresto, M. G. De Paola, and V. Calabrò, "Importance of the properties, collection, and storage of waste cooking oils to produce high-quality biodiesel – An overview," *Biomass and Bioenergy*, vol. 189, 2024, Art. no. 107363, doi: 10.1016/j.biombioe.2024.107363.

[39] X. Cao, X. Li, N. Shu, C. P. Tan, Y.-J. Xu, and Y. Liu, "The characteristics and analysis of polar compounds in deep-frying oil: A mini review," *Food Analytical Methods*, vol. 15, no. 10, pp. 2767–2776, Oct. 2022, doi: 10.1007/s12161-022-02335-x.

[40] Z. Guermat, Y. Kabar, F. Kuznik, and T. E. Boukelia, "Numerical investigation of the integration of new bio-based PCM in building envelopes during the summer in Algerian cities," *Journal of Energy Storage*, vol. 79, 2024, Art. no. 110111, doi: 10.1016/j.est.2023.110111.

[41] M. Abdolahimoghadam and M. Rahimi, "New hybrid nano- and bio-based phase change material containing graphene-copper particles hosting beeswax-coconut oil for solar thermal energy storage: Predictive modeling and evaluation using machine learning," *Energy*, vol. 307, 2024, Art. no. 132604, doi: 10.1016/j.energy.2024.132604.

[42] B. Prabhu et al., "Conch shell derived bio-carbon/paraffin as novel composite phase change material with enhanced thermal energy storage properties for photovoltaic module cooling systems," *Solar Energy Materials and Solar Cells*, vol. 281, 2025, Art. no. 113306, doi: 10.1016/j.solmat.2024.113306.

[43] K. Sato, "Crystallization behaviour of fats and lipids – A review," *Chemical Engineering Science*, vol. 56, no. 7, pp. 2255–2265, Apr. 2001, doi: 10.1016/S0009-2509(00)00458-9.

[44] A. Lazaro et al., "Intercomparative tests on phase change materials characterisation with differential scanning calorimeter," *Applied Energy*, vol. 109, pp. 415–420, Sep. 2013, doi: 10.1016/j.apenergy.2012.11.045.

[45] C. Barreneche, A. Solé, L. Miró, I. Martorell, A. I. Fernández, and L. F. Cabeza, "Study on differential scanning calorimetry analysis with two operation modes and organic and inorganic phase change material (PCM)," *Thermochimica Acta*, vol. 553, pp. 23–26, Feb. 2013, doi: 10.1016/j.tca.2012.11.027.

[46] M. Gao, S. Zhao, H. Yang, X. Wu, and Y. Xiao, "An analysis of the influence of DSC

parameters on the measurement of the thermal properties of phase-change material," *Materials*, vol. 17, no. 23, 2024, Art. no. 5689, doi: 10.3390/ma17235689.

[47] H. Fatahi, J. Claverie, and S. Poncet, "Thermal characterization of phase change materials by differential scanning calorimetry: A review," *Applied Sciences*, vol. 12, no. 23, 2022, Art. no. 12019, doi: 10.3390/app122312019.